Songklanakarin J. Sci. Technol.
40 (3), 484-491, May - Jun. 2018

http://www.sjst.psu.ac.th

Original Article

A simple synthesis and characterization of $LaMO_3$ (M=Al, Co, Fe, Gd) perovskites via chemical co-precipitation method

Wankassama Haron[1], Anurat Wisitsoraat[2], Uraiwan Sirimahachai[1], and Sumpun Wongnawa[1*]

[1] *Department of Chemistry, Faculty of Science, Prince of Songkla University, Hat Yai, Songkhla, 90112 Thailand*

[2] *Nanoelectronics and MEMS Laboratory, National Electronics and Computer Technology Center, Khlong Luang, Pathum Thani, 12120 Thailand*

Received: 14 November 2016; Revised: 18 January 2017; Accepted: 30 January 2017

Abstract

Nanocrystalline $LaMO_3$ (M = Al, Fe, Co, Gd) perovskites were synthesized by the co-precipitation method using metal nitrate and carbonate salts as starting materials. The products were characterized with X-ray diffractometer (XRD), energy-dispersive X-ray spectrometer (EDX), scanning electron microscopy (SEM), transmission electron microscopy (TEM), Brunauer-Emmett-Teller (BET) specific surface area measurement, and UV-vis diffuse reflectance spectroscopy (DRS). The XRD patterns confirmed the formation of the perovskite phase. The SEM micrographs indicated that perovskite samples were nanosized particles with morphology containing porosity due to inter-particle voids. The measured pH_{pzc} of $LaAlO_3$, $LaCoO_3$, $LaFeO_3$, and $LaGdO_3$ in this work were 8.6, 9.2, 9.0, and 8.1, respectively. From the DRS spectra, the band gap energies of $LaAlO_3$, $LaCoO_3$, $LaFeO_3$, and $LaGdO_3$ were calculated as 2.60, 1.50, 2.00, and 2.90 eV, respectively. The preparation of $LaMO_3$ (M = Al, Fe, Co, Gd) perovskites in this work have several advantages such as simplicity, low cost, and no waste compared with other methods.

Keywords: La-based perovskite, $LaAlO_3$, $LaCoO_3$, $LaFeO_3$, $LaGdO_3$, chemical co-precipitation method

1. Introduction

Perovskite is a mixed oxide of transition metals with the chemical formula ABO_3 where A is a transition metal or lanthanide series cation, B is a transition metal cation, and O is an oxide anion (Farhadi *et al*., 2010). The structure of perovskite is a face-centered cubic cell of cation A and anion O. In the unit cell, A locates at the cubic corner and B is at the center of the lattice (Athayde *et al*., 2016). Several properties such as structure, electronics, and magnetic properties of these compounds depend on the types of cations A and B. The properties and uses must be considered hand-in-hand, for example, a perovskite as a gas sensor should have A and B such that ABO_3 exhibits an electronic property as a semi-conductor or if the aim is in fuel cell technology the selected ABO_3 should have a high k dielectric property.

The La-based perovskites of $LaMO_3$ (M=Al, Co, Fe, Gd) are very interesting compounds and they have applications in many fields. $LaAlO_3$ can be used as thermo-luminescent dosimeter (Hernandez *et al*., 2016) and photo-luminescense material (Alves *et al*., 2014; Fu *et al*., 2016), while $LaCoO_3$ finds applications in the field of catalysts (Pang *et al*., 2016), fuel cells (Natile *et al*., 2017), and gas sensors (Ding *et al*., 2015; Shi *et al*., 2015). The $LaFeO_3$ perovskite has been studied as a photocatalyst (Kumar *et al*., 2017), gas sensor (Cao *et al*., 2017; Chen *et al*., 2016; Wei *et al*., 2017), and cathode for fuel cells (Choi *et al*., 2016). $LaGdO_3$ can be used as a dielectric material for pulse lasers (Pavunny *et al*., 2011) and as a high k dielectric material in electronic devices (Pavunny *et al*., 2014). The efficiency of these materials

*Corresponding author
Email address: sumpun.w@psu.ac.th

depends on the synthesis method (Athayde *et al*., 2016). Many methods are available for the synthesis of perovskite oxides in the group of La-based perovskites such as solid state reaction (Rodriguez *et al*., 2017), sol gel (Cao *et al*., 2017), solution combustion synthesis (Fu *et al*., 2016), electrospinning (Li *et al*., 2016), hydrothermal synthesis (Niu *et al*., 2016), co-precipitation methods (Chandradass *et al*., 2014; Tompsett *et al*., 1998), EDTA-glycine process (Qin *et al*., 2013), and reverse microemulsion process (Tian *et al*., 2009). These techniques, however, still have disadvantages that involve several steps and sometimes require more than the necessary starting reagents.

Our research group attempted to study the preparation of La-based oxide of nano-$LaMO_3$ perovskites via a simple co-precipitation method and investigated their inherited properties for further applications. In this study, 4 types of M (metal group 3A (Al as Al^{3+}), transition metals (Co as Co^{2+} or Co^{3+} and Fe as Fe^{3+}), and a lanthanide metal (Gd as Gd^{3+})) were covered. In 2014 and 2015 we reported preliminary results on the syntheses and characterizations of $LaAlO_3$ and $LaFeO_3$ (Haron *et al*., 2014, 2015). In this article, more details are reported on the syntheses and characterizations of $LaAlO_3$ and $LaFeO_3$ with an extension to cover Co and Gd. Compared with other routes, the synthesis route we describe has several advantages, such as simplicity, low cost, and no waste, that we deem would be useful for others who are beginning to work in this field.

2. Materials and Methods

2.1 Syntheses of $LaMO_3$ perovskites

$LaMO_3$ (M = Al, Co, Fe, Gd) perovskites were prepared with some modifications based on the co-precipitation method reported previously (Villoria *et al*., 2011). $La(NO_3)_3{\cdot}6H_2O$ and $Al(NO_3)_3{\cdot}6H_2O$ were used as the starting materials for preparation of $LaAlO_3$. A specified amount of each was dissolved in distilled water to make 1 M solutions and mixed together with vigorous stirring. Then an aqueous solution of $K_2CO_3{\cdot}1.5H_2O$ (2 M) – same volume as the nitrate solution – was rapidly added. A small amount of NaOH solution (1 M) was introduced to initiate precipitation. After the precipitation was complete, the precipitate was filtered and washed with distilled water several times until the washed water became neutral (pH = 7). The product was then dried at 100 °C for 6 h to yield the "precursor" after which it was calcined at 700, 800, and 900 °C for 2 h to obtain the $LaAlO_3$ perovskite.

For $LaCoO_3$, $LaFeO_3$, and $LaGdO_3$ perovskites, the same procedure as above was applied but with $Co(NO_3)_2{\cdot}6H_2O$, $Fe(NO_3)_3{\cdot}9H_2O$, and $Gd(NO_3)_3{\cdot}6H_2O$ as the starting materials, respectively. Each precursor then was calcined at planned temperatures for 2 h: $LaCoO_3$ at 200, 400, 600 °C, $LaFeO_3$ at 600, 700, 800 °C, and $LaGdO_3$ at 1000, 1100, 1200 °C.

2.2 Characterization techniques

The crystalline phases of the $LaMO_3$ (M=Al, Co, Fe, Gd) samples were investigated using an X-ray powder diffractometer, Philips PW 3710 (PHILIPS X' Pert MPD) employing Cu Kα (λ = 0.154 nm) radiation and a Ni filter, over the range of 2θ = 20−80°. The average crystallite size (D) was calculated with the Debye-Scherrer equation, Equation (1),

$$D = \frac{K\lambda}{B.\cos\theta} \quad (1)$$

where D is the average crystallite size, K is a dimensionless shape factor with a typical value of about 0.89 but may vary with the actual shape of the crystallite. The λ is the X-ray wavelength, B is the line width at half the maximum intensity after subtracting the instrumental line broadening in radians, and θ is the Bragg angle. The metal constituents of $LaMO_3$ perovskites were investigated by using energy-dispersive X-ray spectrometer (EDX), ISIS 300, Oxford, England. The morphology of the $LaMO_3$ particles was examined using scanning electron microscopy (SEM) (JEOL, JSM-5800 LV) operated at 20 kV in secondary electron imaging mode and transmission electron microscopy (TEM) (JEOL, JSM-2010) operated at 200 kV in bright-field mode. The specific surface area and pore size distribution were determined by nitrogen sorption isotherm using the Brunauer-Emmett-Teller (BET) method (Coulter, Model SA3100, USA).

2.3 Determination of pH at point of zero charge (pH_{pzc})

A sodium chloride solution of 0.1 mol/L was prepared by dissolving an accurately weighed amount of NaCl salt in a 1 L volumetric flask. Several portions of 50 mL of this solution were pipetted and poured into several 250 mL Erlenmeyer flasks. From these solutions, various solutions of pH 1–12 were made using diluted solutions of HCl or NaOH and recorded as initial pH, pH_i (Liao *et al*., 1999).

About 0.05 g of $LaMO_3$ was added into each flask and sealed with constant agitation using a magnetic stirrer for 24 h. The stirring rate was controlled at 300 rpm. At the end of the experiment, the equilibrated solutions were decanted and the pH was measured as the final pH, pH_f. A graph was constructed by plotting pH_i against pH_f and the pH_{pzc} was determined from the crossover point of pH_i and pH_f in the graph.

2.4 UV-vis diffuse reflectance spectroscopy (DRS)

The UV-vis diffuse reflectance spectra (DRS) were recorded from 200 nm to 800 nm. The band gap energy was then calculated using the Kubelka-Munk equation:

$$(Rh\nu)^2 = A\,(h\nu - Eg) \quad (2)$$

where R is the absorbance, hν is the absorption energy, A is the parameter related to the effective masses associated with the valence and conduction bands, n is refraction index, and Eg is the band gap energy (Stampler *et al*., 2008).

3. Results and Discussion

3.1 Syntheses of $LaMO_3$ products

For M = Al, Co, Fe, and Gd, the colors of the precursors obtained in the first stage were white, violet, brown, and white, respectively. After calcination at 900 (M=Al), 600

(M=Co), 800 (M=Fe), and 1200 °C (M=Gd) for 2 h, the precursors turned to the corresponding perovskites. The colors of the perovskites were white, black, dark brown, and white, respectively. Photographs showing the colors of the precursors and perovskites are displayed in Figure 1.

Figure 1. Precursors prepared by the chemical co-precipitation method and perovskite oxides after calcinations at 900 °C ($LaAlO_3$), 600 °C ($LaCoO_3$), 800 °C ($LaFeO_3$), and 1200 °C ($LaGdO_3$) for 2 h: (a1) $LaAlO_3$ precursor, (a2) $LaAlO_3$ perovskite, (b1) $LaCoO_3$ precursor, (b2) $LaCoO_3$ perovskite, (c1) $LaFeO_3$ precursor, (c2) $LaFeO_3$ perovskite, (d1) $LaGdO_3$ precursor, and (d2) $LaGdO_3$ perovskite.

In this study, $LaMO_3$ (M = Al, Co, Fe, Gd) perovskite powders were prepared by the co-precipitation method. The process may be described by the following chemical reactions.

$$2\ La(NO_3)_3 + 2\ M(NO_3)_3 + 6\ K_2CO_3 \longrightarrow La_2(CO_3)_3 + M_2(CO_3)_3 + 12\ KNO_3$$

$$La_2(CO_3)_3 + M_2(CO_3)_3 \xrightarrow{\text{high temp 1}} La_2O_3 + M_2O_3 + 6CO_2$$

$$La_2O_3 + M_2O_3 \xrightarrow{\text{high temp 2}} 2\ LaMO_3$$

where M = Al, Co, Fe, Gd; high temp 2 > high temp 1.

The precursor first obtained was a mixture of $La_2(CO_3)_3$ and $M_2(CO_3)_3$ which later was subjected to calcination. As the temperature rose, the carbonates decomposed to the corresponding oxides and subsequently transformed to the corresponding perovskite at high temperature.

3.2 Product characterizations

3.2.1 X-ray diffractometer (XRD)

The formation of oxides prior to formation of the perovskite phase was evidenced from the XRD patterns displayed in Figures 2 and 3. For $LaAlO_3$, the perovskite phase was detected only at 900 °C (Figure 2a). At temperatures lower than 900 °C, the products were mixtures of La_2O_3 and Al_2O_3. The XRD peaked at 900 °C which matched the hexagonal structures of $LaAlO_3$ perovskite (JCPDS file no. 85-0848). The average crystallite size of this $LaAlO_3$ was 75 nm using Equation (1).

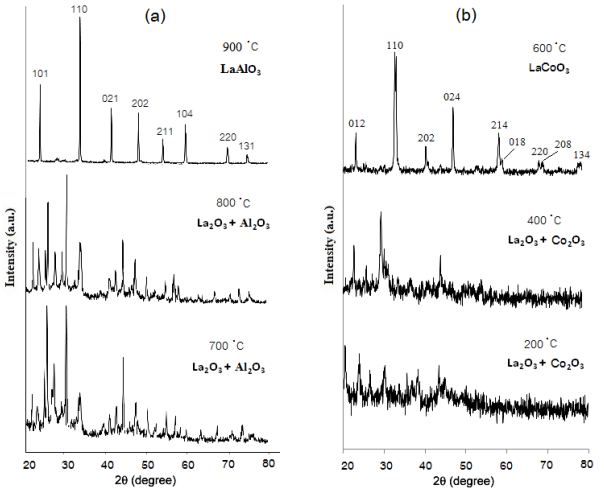

Figure 2. XRD patterns of products from (a) $LaAlO_3$ and (b) $LaCoO_3$ obtained from various calcination temperatures for 2 h.

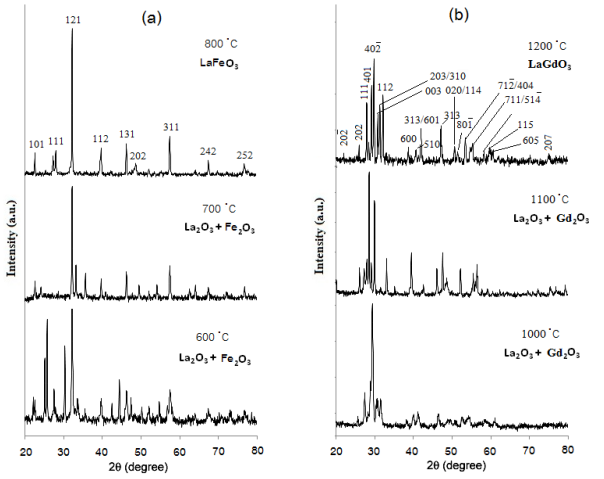

Figure 3. XRD patterns of (a) $LaFeO_3$ and (b) $LaGdO_3$ obtained from various calcination temperatures for 2 h.

The XRD patterns of $LaCoO_3$ and $LaFeO_3$ obtained at various temperatures are shown in Figures 2b and 3a. For $LaCoO_3$, the initial +2 charge was oxidized by oxygen during the heating stage to +3. The rhombohedral $LaCoO_3$ perovskite formed at 600 °C matched JCPDS file no. 48-0123. Otherwise, a mixture of La_2O_3 and Co_2O_3 was obtained if the calcination temperature was lower than 600 °C. The crystallite size of $LaCoO_3$ at 600 °C was 69 nm. For $LaFeO_3$, the product obtained from calcination at 800 °C was $LaFeO_3$ perovskite which matched JCPDS file no. 37-1493 having an orthorhombic structure with crystallite size of 68 nm. If the calcination temperature was lower than 800 °C, only a mixture of La_2O_3 and Fe_2O_3 was obtained.

The perovskite phase of $LaGdO_3$ was formed at a very high temperature. From the XRD pattern, the $LaGdO_3$, perovskite phase was detected only at 1200 °C. At lower than 1200 °C, the products were mixtures of La_2O_3 and Gd_2O_3. The XRD pattern of $LaGdO_3$ at 1200 °C matched JCPDS file no. 42-1465 of a monoclinic $LaGdO_3$ structure (Figure 3b). The XRD peak information yielded an average crystallite size of 71 nm.

The appearances of XRD patterns of all four perovskites were sufficiently clean from other unwanted peaks. Therefore, it can be considered that the methods used were able to produce the perovskite phase without waste compared with other methods.

The syntheses using the low temperature not only saved energy but also increased the surface area of the perovskite products. Varying the calcination temperature for the synthesis $LaFeO_3$ was reported in 2015 from our group (Haron *et al*., 2015), while the same information of $LaAlO_3$, $LaCoO_3$, and $LaGdO_3$ has not appeared in the literature. Hence, this research is the first to provide this information. The results of $LaFeO_3$ in this article were from the reinvestigation carried out simultaneously with the other three perovskites and still bear resemblance to the report in 2015.

3.2.2 Energy dispersive x-ray spectrometer (EDX)

The purity of each sample was also checked with EDX spectrometer (Figure 4). From the EDX pattern, all the elements detected were those that were expected to be present in the samples, i.e. La, Al, Co, Fe, Gd, and O. In addition, all powder samples contained insignificant amounts of other contaminating elements which affirmed a high purity of the synthesized perovskite oxides.

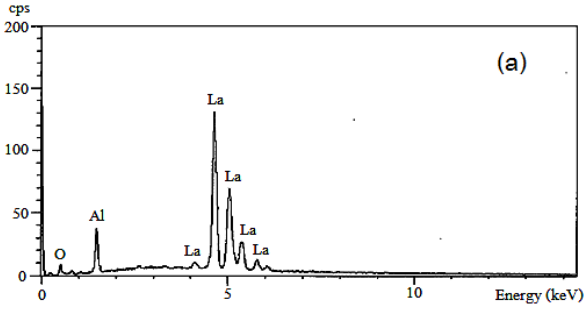

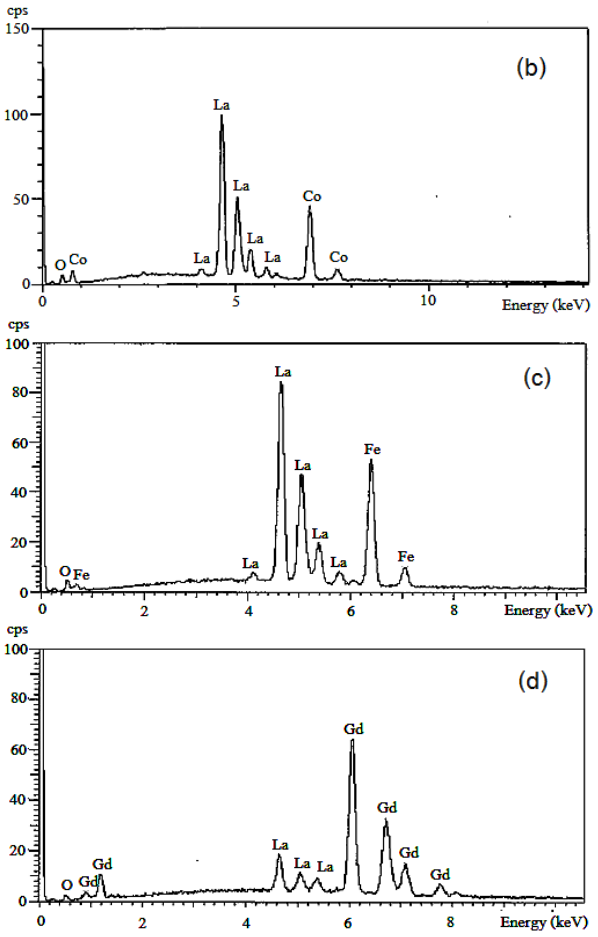

Figure 4. EDX spectra of (a) $LaAlO_3$, (b) $LaCoO_3$, (c) $LaFeO_3$, and (d) $LaGdO_3$ powders prepared by co-precipitation after calcination at 900, 600, 800, and 1200 °C.

3.2.3 Scanning electron microscopy (SEM)

The morphologies of all samples were investigated using scanning electron microscopy (SEM). Figure 5 shows the SEM micrographs of the $LaMO_3$. It can be seen clearly that each sample at 10,000 and 30,000 magnifications has its own characteristic morphology. The surface of $LaAlO_3$ appeared as a mixture of 2 types of grains of cubic shape and nanorod-like shape. The cubics and short sticks aggregated to become clusters with some porosity. The nanorods were >1 μm in length with thicknesses of approximately 10 nm and widths in the range of 10−100 nm. These grain shapes caused the porosity which should be beneficial in applications such as gas sensors and metal ion adsorbents (Figure 5a). In contrast, the SEM image of the $LaCoO_3$ perovskite revealed that its surface was composed of small grains with round shapes and the surface was very smooth (Figure 5b). The $LaFeO_3$ perovskite exhibited large amounts of round grains mixed with small amounts of stick grains (Figure 5c). The round grains of $LaFeO_3$ were small but they were bigger than the round grains of $LaCoO_3$. On the other hand, $LaGdO_3$ existed as large long grain shapes (length >2 μm) that were the largest compared with $LaAlO_3$, $LaCoO_3$, and $LaFeO_3$.

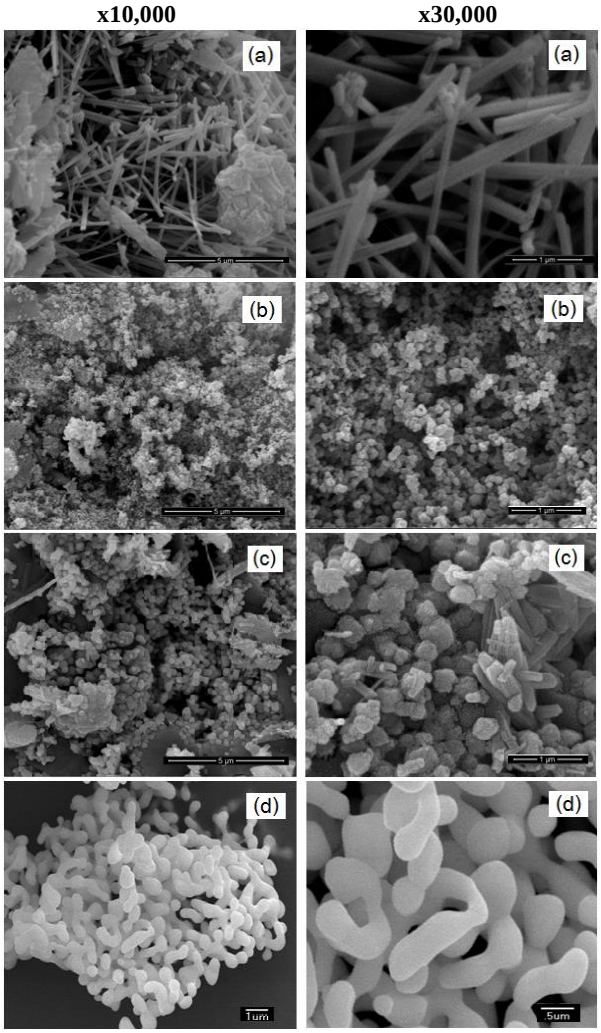

Figure 5. SEM images at x10,000 and x30,000 magnifications of (a) $LaAlO_3$, (b) $LaCoO_3$, (c) $LaFeO_3$, and (d) $LaGdO_3$ powders prepared by the co-precipitation method.

The surface morphologies of the $LaMO_3$ (M = Al, Co, Fe, Gd) perovskites found in this work were both similar to and different from those previously reported by other groups. Li *et al*., 2007 studied the SEM of $LaAlO_3$ synthesized by the molten salt route at 800 °C for 3 h. The surface of their sample had extended cubic shaped particles similar to the surface of as-synthesized $LaAlO_3$ in this work. For $LaCoO_3$ prepared by other methods, the particle morphologies of $LaCoO_3$ were micron size with a high degree of agglomeration composed of nanocrystallites with an average size of 11 nm (Ghasdi *et al*., 2010). Wang *et al*., 2013 studied the microstructure of $LaFeO_3$ powders prepared by sol gel method and calcined at 800 °C for 2 h. The SEM of the sample contained grains with large particles accompanied by smoother surfaces. In the case of $LaGdO_3$, no information has been found in the literature for comparison.

3.2.4 Transmission electron microscope (TEM)

From the TEM micrographs (Figure 6), $LaAlO_3$ appeared as porous material composed of nanorods containing internal pores throughout the structure (Figure 6a). The pore diameters were in the range of 10−80 nm. This unique feature may provide additional benefit from the surface area for applications in gas sensor, catalyst, and metal ion adsorption. $LaCoO_3$, which was also a porous material, had round grains (Figure 6b), while $LaFeO_3$ had stick-shaped grains with round edges (Figure 6c). The last member of the group, $LaGdO_3$, exhibited very large grains which were the largest of all four as-synthesized perovskites in this set (Figure 6d).

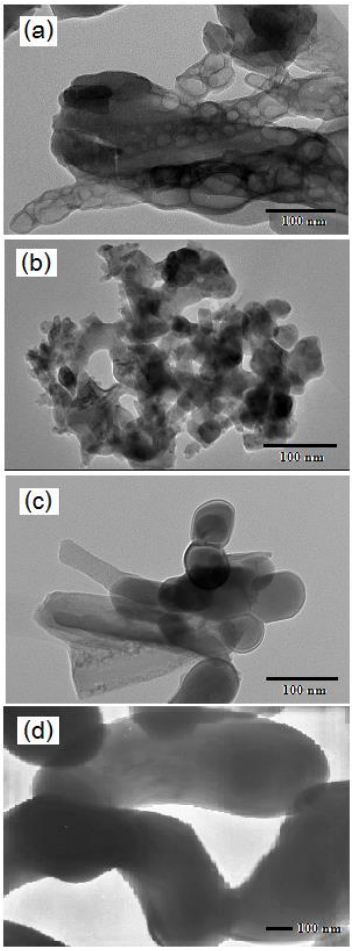

Figure 6. TEM images of (a) $LaAlO_3$, (b) $LaCoO_3$, (c) $LaFeO_3$, and (d) $LaGdO_3$ powders prepared by co-precipitation.

3.2.5 Specific surface area measurement

The BET surface area and pore volume of $LaMO_3$ at difference calcination temperatures based on the N_2 adsorption isotherms are given in Table 1. It can be seen that the nano $LaAlO_3$ had the highest surface area at 61.7 m^2/g, while both nano-$LaCoO_3$ and $LaFeO_3$ had almost identical

Table 1. BET surface area and total pore volume of $LaMO_3$ (M=Al, Co, Fe, Gd) prepared by the co-precipitation method.

Perovskite $LaMO_3$	Calcined temp. (°C)	Total pore volume (cc/g)	Surface area (m^2/g)	Surface area reported in the literature (m^2/g)
$LaAlO_3$	900	0.13	61.7	43.0 (Negahdari *et al.*, 2009)
$LaCoO_3$	600	0.06	23.1	27.0 (Farhadi *et al.*, 2010)
$LaFeO_3$	800	0.07	23.0	36.5 (Farhadi *et al.*, 2009)
$LaGdO_3$	1200	0.03	5.4	No data

surface areas of about 23 m^2/g which was similar to those reported in the literature. Since both Co^{3+} and Fe^{3+} have equal ionic radii (=60 pm), that could be the reason for the equal surface areas of $LaCoO_3$ and $LaFeO_3$. The surface area of $LaGdO_3$ was 5.4 m^2/g, which was the lowest in the $LaMO_3$ group. This could be the result of the large Gd^{3+} ionic size (93.5 pm) and its high atomic weight, hence, fewer unit cells per gram and low surface area per gram.

The surface areas of the synthesized $LaAlO_3$, $LaCoO_3$ and $LaFeO_3$ were not much different from those reported by other researchers (Table 1). No data has been previously reported for $LaGdO_3$.

3.3 pH at point of zero charge (pH_{pzc})

The pH_{pzc} determinations were carried out using the pH drift method (Liao *et al.*, 1999). The equilibrated pH (pH_f) of the as-synthesized $LaMO_3$ (M = Al, Co, Fe, Gd) perovskites were plotted against the initial pH (pH_i) of the solution having a constant ionic strength (0.1 mol/L NaCl). The pH at the point where the initial pH of the solution crossed over the equilibrated pH is the pH_{pzc} of the sample (Figure 7a-c). The measured pH_{pzc} of $LaAlO_3$ (Figure 7a), $LaCoO_3$ (Figure 7b), $LaFeO_3$ (Figure 7c), and $LaGdO_3$ (Figure 7d) in this work were 8.6, 9.2, 9.0, and 8.1, respectively, indicating the surfaces of all synthesized $LaMO_3$ were slightly basic. The pH_{pzc} of $LaAlO_3$ and $LaCoO_3$ in this work were not much different from those reported at 9.9 (Negahdari *et al.*, 2009) and 12.8 (Mezaini *et al.*, 2014), respectively. No published data are available for $LaFeO_3$ and $LaGdO_3$.

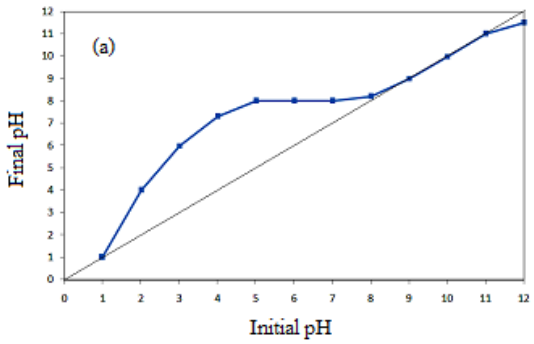

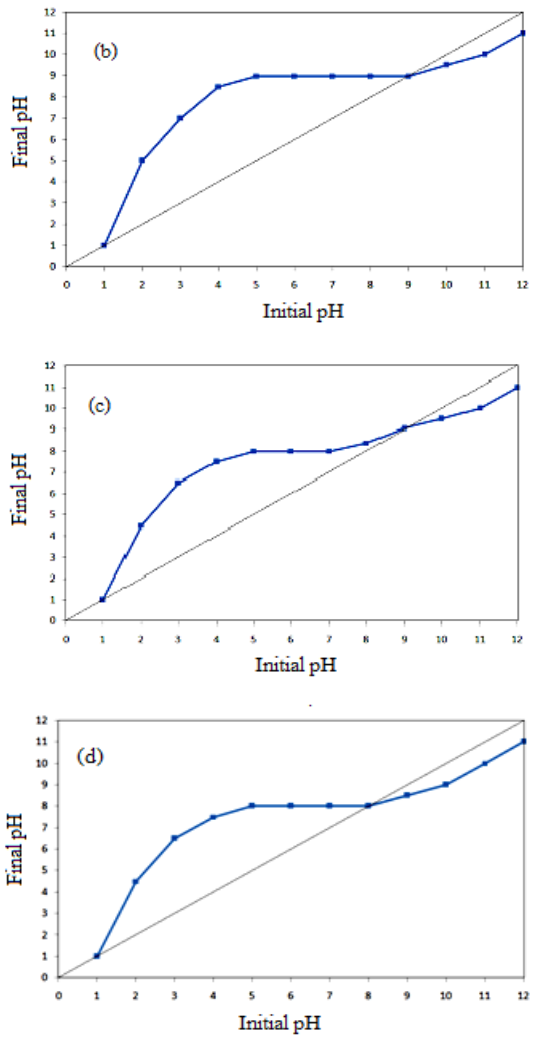

Figure 7. Plots for the determination of pHpzc of (a) LaAlO3, (b) LaCoO3, (c) LaFeO3, and (d) LaGdO3.

3.4 UV-vis diffuse reflectance spectroscopy (DRS)

For the DRS spectra of $LaMO_3$ (M = Al, Co, Fe, Gd) in the range of 200–800 nm, the details of spectra were observable only in the range of 200–400 nm for all samples. The band gap energy was calculated using the Kubelka-Munk (Figure 8a-c) and the obtained band gap energies of $LaAlO_3$, $LaCoO_3$, $LaFeO_3$, and $LaGdO_3$ were 2.60, 1.50, 2.00, and 2.90 eV respectively. This result confirmed that all $LaMO_3$ perovskites were all semiconductor materials.

Materials for applications such as gas sensor and heavy metal adsorbent should be a porous nanomaterial with a high surface area and be a semiconductor (for gas sensor). $LaAlO_3$ from this work is a nanocrystalline perovskite with the highest surface area among the perovskites synthesized as well as being a semiconductor material. These properties put $LaAlO_3$ as the most promising candidate for further investigation in the area of gas sensor and metal ion adsorption for wastewater treatment.

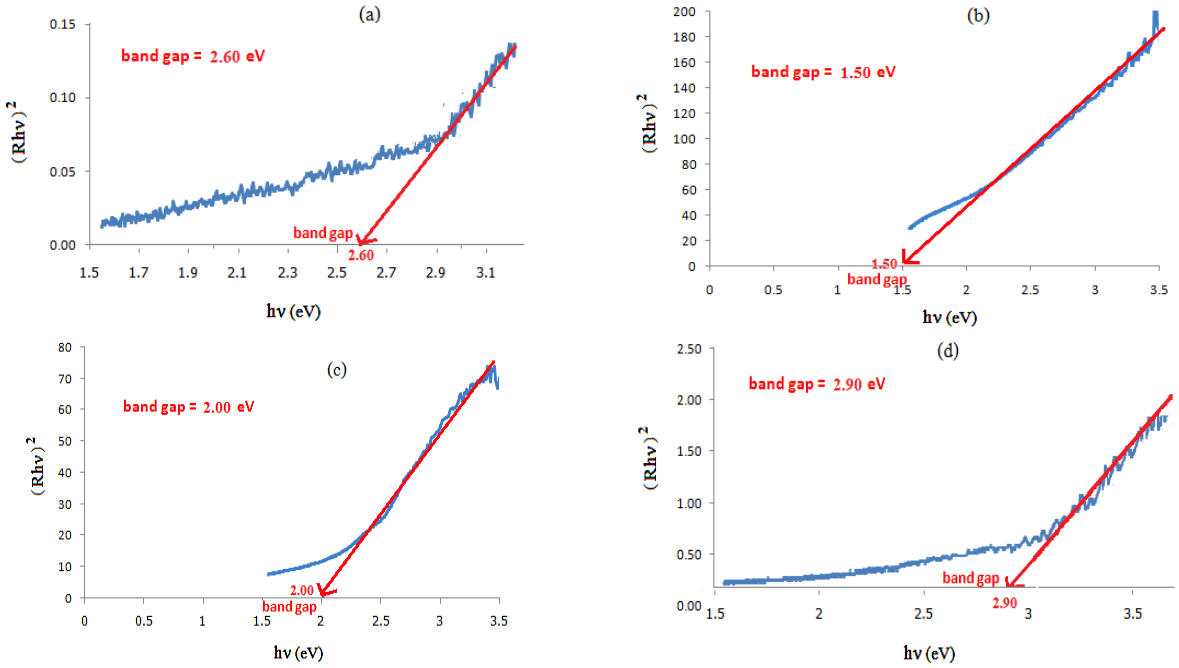

Figure 8. Band gap energy determinations using the Kubelka-Munk plot for (a) $LaAlO_3$, (b) $LaCoO_3$, (c) $LaFeO_3$, and (d) $LaGdO_3$.

4. Conclusions

Nanocrystalline $LaMO_3$ (M = Al, Co, Fe, Gd) perovskites in powder form were prepared using the co-precipitation method at lower calcination temperatures, i.e. lower than conventional methods. The products were characterized with XRD, EDX, SEM, TEM, and BET which revealed significant differences in physical properties of the samples. We found that $LaAlO_3$ showed very interesting properties among the four perovskites prepared such as the high surface area and semiconductor properties with a band gap =2.60 eV. We hope that from this work the synthesized $LaAlO_3$ will be a standout in applications such as a gas sensing material and heavy metal ion adsorbent. The syntheses of $LaMO_3$ (M = Al, Co, Fe, Gd) perovskites in this work have several advantages such as simplicity, low cost, and no waste compared with other methods. Parts of the data that appear in this report are the first ever to be reported.

Acknowledgements

The authors wish to acknowledge the Office of the Higher Education Commission of Thailand (OHEC) and the Graduate School, Prince of Songkla University, Thailand for the financial support of this work.

References

Alves, N., Ferraz, W. B., & Faria, L. O. (2014). Synthesis and investigation of the luminescent properties of carbon doped lanthanum aluminate ($LaAlO_3$) for application in radiation dosimetry. *Radiation Measurements, 71*, 90-94.

Athayde, D. D., Souza, D. F., Silva, A. M. A., Vasconcelos, D., Nunesa, E. H. M., Costa, J. C. D., & Vasconcelos, W. L. (2016). Review of perovskite ceramics synthesis and membrane preparation methods. *Ceramics International, 42*, 6555-6571.

Cao, E., Yang, Y., Cui, T., Zhang, Y., Hao, W., Sun, L., . . . Deng, X. (2017). Effect of synthesis route on electrical and ethanol sensing characteristics for $LaFeO_{3-\delta}$ nanoparticles by citric solgel method. *Applied Surface Science, 393*, 134-143.

Chandradass, J., Kim, H., & Momadec, F. W. Y. (2014). Effect of different solvents in the synthesis of $LaCoO_3$ nanopowders prepared by the co-precipitation method. *Advanced Powder Technology, 25*, 1834-1838.

Chen, Y., Qin, H., Wang, X., Li, L., & Hu, J. (2016). Acetone sensing properties and mechanism of nano$LaFeO_3$ thick films. *Sensors and Actuators B: Chemical, 235*, 56-66.

Choi, J., Kim, B., Song, S. H., Park, J. S. (2016). A composite cathode with undoped $LaFeO_3$ for protonic ceramic fuel cells. *International Journal of Hydrogen Energy, 41*, 9619-9626.

Ding, J. C., Li, H. Y., & Guo, X. (2015). CO sensing mechanism of $LaCoO_3$. *Solid State Ionics, 272*, 155-159.

Farhadi, S., & Sepahvand, S. (2010). Microwave-assisted solid-state decomposition of La $[Co(CN)_6]\cdot 5H_2O$ precursor: A simple and fast route for the synthesis of single phase perovskite-type $LaCoO_3$ nano-particles. *Journal of Alloys Compounds, 489*, 586-591.

Fu, Z., & Liu, B. (2016). Solution combustion synthesis, photoluminescence and X-ray luminescence of Eu^{3+} -doped $LaAlO_3$ nanophosphors. *Ceramics International, 42*, 2357-2363.

Ghasdi, M., & Alamdari, H. (2010). CO sensitive nanocrystalline $LaCoO_3$ perovskite sensor Prepared by high energy ball milling. *Sensors and Actuators B: Chemical, 148*, 478–485.

Hernandez, A. M., Medina, J. Z., Garcia, M. E. C., Nieto, J. A., & Montalvo, T. R. (2016). Synthesis and thermoluminescence of $LaAlO_3:Pr^{3+}$ to UVC radiation dosimetry. *Applied Radiation and Isotopes, 118*, 12-17.

Haron, W., Wisitsoraat, A., & Wongnawa, S. (2014). Comparison of nanocrystalline $LaMO_3$ (M = Co, Al) perovskite oxide prepared by coprecipitation method. *International Journal of Chemical Engineering and Applications, 5*, 123-126.

Haron, W., Wisitsoraat, A., & Wongnawa, S. (2015). Nanocrystalline $LaFeO_3$ perovskite oxide prepared at lower temperature with improved ethanol gas sensoring. *Proceeding of the Int'l Conference on Biotechnology, Nanotechnology and Environmental Engineering (ICBNE)*, 10-14. Retrieved from http://iaast.org/upload/1624A0415053.pdf

Kumar, R. D., Thangappan, R., & Jayavel, R. (2017). Synthesis and characterization of $LaFeO_3/TiO_2$ nanocomposites for visible light photocatalytic activity. *Journal of Physics and Chemistry of Solids, 101*, 25-33.

Li, Z., Zhang, S., & Lee, W. E. (2007). Molten salt synthesis of $LaAlO_3$ powder at low temperatures. *Journal of the European Ceramic Society, 27*, 3201–3205.

Li, S., Zhao, Y., Wang, C., Li, D., & Gao, K. (2016). Fabrication and characterization unique ribbonlike porous $Ag/LaFeO_3$ nanobelts photocatalyst via electrospinning. *Materials Letters, 170*, 122-125.

Liao, H. K., Chi, L. L., Chou, J. C., Chung, W. Y., Sun, T. P., & Hsiung, S. K. (1999). Study on pH_{pzc} and surface potential of tin oxide gate ISFET. *Materials Chemistry and Physics, 59*, 6-11.

Natile, M. M., Egerb, G., Batocchic, P., Mauvyc, F., & Glisentia, A. (2017). Strontium and copper doped $LaCoO_3$: New cathode materials for solid oxide fuel cells. *International Journal of Hydrogen Energy, 42*(3), 1724-1735.

Niu, T., Liu, G. L., Chen, Y., Yang, J., Wu, J., Cao, Y., & Liu, Y. (2016). Hydrothermal synthesis of graphene $LaFeO_3$ composite supported with CuCo nanocatalyst for higher alcohol synthesis from syngas. *Applied Surface Science, 364*, 388-399.

Pang, X., Guo, Y., Zhang, Y., Xub, B., & Qia, F. (2016). $LaCoO_3$ perovskite oxide activation of peroxymonosulfate for aqueous 2phenyl5sulfobenzimidazole degradation: Effect of synthetic method and the reaction mechanism. *Chemical Engineering Journal, 304*, 897-907.

Pavunny, S. P., Thomas, R., Kumar, A., Murari, N. M., & Katiyar, R. S. (2011). Dielectric properties and electrical conduction of high-k $LaGdO_3$ ceramics. *Journal of Applied Physics, 111*, 102811-102816.

Pavunny, S. P., Scott, J. F., & Katiyar, R. S. (2014). Lanthanum gadolinium oxide: A new electronic device material for CMOS logic and memory devices. *Materials, 7*, 2669-2696.

Qin, G., Huang, X., Chen, J., & He, Z. (2013). Synthesis of Sr and Mg double-doped $LaAlO_3$ nanopowders via EDTA-glycine combined process. *Powder Technology, 235*, 880-885.

Rodriguez, D. S., Wada, H., Yamaguchi, S., Farjas, J., & Yahiro, H. (2017). Synthesis of LaFeO3 perovskite-type oxide via solid-state combustion of a cyano complex precursor: The effect of oxygen diffusion. *Ceramics International, 43*, 3156-3165.

Shi, C., Qin, H., Li, L., Chen, Y., Ju, L, & Hu, J. (2015). CO_2 sensing characteristics and mechanism for $LaCoO_3$ predicted by density function theory. *Applied Surface Science, 327*, 168-173.

Stampler, E. S., Sheets, W. C., Bertoni, M. I., Prellier, W., Mason, T. O., & Poeppelmeier, K. R. (2008). Temperature driven reactant solubilization synthesis of BiCuOSe. *Inorganic Chemistry, 47*, 10009-10016.

Tian, Z., Huang, W., & Liang, Y. (2009). Preparation of spherical nanoparticles of $LaAlO_3$ via the reverse microemulsion process. *Ceramic International, 35*, 661-664.

Tompsett, G. A., Phillips, R. J., Sammes, N. M., & Cartner, A. M. (1998). Characterisation of $LaGdO_3$ by X-ray powder diffraction and Raman spectroscopy. *Solid State Communications, 108*, 655-660.

Villoria, JA., Alvarez-Galvana, MC., Al-Zahranib, SM., Palmisanoc, P., Specchiac, S., Specchiac, V, (2011). Oxidative reforming of diesel fuel over. $LaCoO_3$ perovskite derived catalysts: Influence of perovskite synthesis method on catalyst properties and performance. *Applied Catalysis B: Environmental, 105*, 276-288.

Wang, X., Qin, H., Sun, L., & Hu, (2013). CO_2 sensing properties and mechanism of nanocrystalline $LaFeO_3$ sensor. *Sensors and Actuators B: Chemical, 188*, 965-971.

Wei, W., Guo, S., Chen, C., Sun, L., Chen, Y., Guo, W., & Ruan, S. (2017). High sensitive and fast formaldehyde gas sensor based on Ag doped $LaFeO_3$ nanofibers. *Journal of Alloys and Compounds, 695*, 1122-1127.